Hyperspectral complex domain denoising

Vladimir Katkovnik, Igor Shevkunov, Karen Egiazarian
Faculty of Information Technology and Communication Sciences, Computational Imaging Group
Tampere University
Tampere, Finland
Email:{vladimir.katkovnik, igor.shevkunov, karen.eguaizarian}@tuni.fi

***Abstract*—We consider hyperspectral complex domain imaging from hyperspectral complex-valued noisy observations. The proposed algorithm is based on singular value decomposition (SVD) of observations and complex domain block-matching 3D (CDBM3D) filtering in optimized SVD eigenspace. Simulation experiments demonstrate high efficiency of the proposed complex domain joint filtering of hyperspectral data in comparison with CDBM3D filtering of separate 2D slices of hyperspectral cubes as well as with respect to joint real domain independent phase/amplitude filtering this kind of data.**

***Index Terms*—Hyperspectral imaging, singular value decomposition, sparse representation, noise filtering, noise in imaging systems**

I. Introduction

Hyperspectral imaging (HSI) is applied in variety of applications, in particular, earth surface remote sensing [1], medical and bio-medical sciences [2]. Typically, HSI retrieves a valuable information based on images obtained across a wide range of electromagnetic spectrum with hundreds to thousands of spectral channels. These images are two-dimensional ($2D$) and stacked together in $3D$ cubes, where (x, y) are transverse spatial coordinates and the third coordinate is for a spectral channel, which usually is represented by wavelength λ.

Complex domain HSI makes a special class of the hyperspectral problems since variables of interest are complex-valued and both phase and amplitude have to be reconstructed. It is a very promising technique which doubles amount of retrieved information in comparison with real-valued HSI, since hyperspectral cubes are complex-valued, i.e. each of the $2D$ images for each wavelength is complex-valued with $2D$ phase and amplitude. Complex-valued hyperspectral (HS) cubes may appear as the Fourier transform of observed real-valued variables (e.g. [3]) or as direct measurements of real and imaginary parts of complex-valued parameters. For instance, in magnetic resonance imaging (MRI) and functional magnetic resonance imaging (fMRI), images or voxel measurements are complex valued (e.g. [4]). Recently, HS digital holography has been developed, which, additionally to the conventional holography, is able to recover a spectrally resolved phase/amplitude information (e.g. [5], [6]).

In many applications, HS cubes are derived from indirect observations as solutions of inverse problems, what leads to a serious noise amplification. A sliding window averaging along wavelength dimension is used routinely for noise suppression (e.g. [5], [6]), but this straightforward technique may result in oversmoothing of details of interest. Some sophisticated algorithms for separate filtering phase and amplitude slices are proved being more efficient for HSI [7].

A novel effective denoising algorithm taking into consideration phase/amplitude correlation between and within slices of HS cubes is a contribution of this paper. We illustrate the performance of the proposed algorithm by simulation experiments, where the clean HS signals are known and the noise in observations is complex-valued circular Gaussian. The developed algorithm is a complex domain version of the real domain HSI algorithm developed in [8].

Academy of Finland, project no. 287150, 2015-2019.

II. Problem formulation

Let $U(x, y, \lambda) \subset \mathbb{C}^{N\times M}$ be a slice $N \times M$ on (x, y) of a complex-valued hyperspectral cube provided a fixed wavelength λ, and $Q_\Lambda(x, y) = \{U(x, y, \lambda),\ \lambda \subset \Lambda\}$, $Q_\Lambda \subset \mathbb{C}^{N\times M\times L_\Lambda}$ be the whole cube composed of the set of the wavelengths Λ with number of individual wavelengths L_Λ.

The total size of the cube is $N \times M \times L_\Lambda$ pixels. The third dimension rows of $Q_\Lambda(x, y)$ contain L_Λ spectral observations corresponding to the scene with fixed coordinates (x, y). Then, the noisy HS observations with the additive noise may be written as:

$$Z_\Lambda(x, y) = Q_\Lambda(x, y) + \varepsilon_\Lambda(x, y), \tag{1}$$

where $Z_\Lambda, Q_\Lambda,\ \varepsilon_\Lambda \subset \mathbb{C}^{N\times M\times L_\Lambda}$ represent noisy HS data, clean HS and additive noise, respectively.

Accordingly to the notation for the clean image, the noisy cube can be represented as $Z_\Lambda(x, y) = \{Z(x, y, \lambda),\ \lambda \in \Lambda\}$, $Z_\Lambda \subset \mathbb{C}^{N\times M\times L_\Lambda}$ with slices $Z(x, y, \lambda)$.

The denoising problem is formulated as reconstruction of unknown $Q_\Lambda(x, y)$ from the given $Z_\Lambda(x, y)$.

The properties of the clean HS cube $Q_\Lambda(x, y)$ and the noise $\varepsilon_\Lambda(x, y)$ are essential for the algorithm development.

The following three assumptions are basic hereafter.

1) *Similarity* of HS slices $U(x, y, \lambda)$ for close values of λ follows from the fact that usually the slides $U(x, y, \lambda)$ are slowly varying on λ. It follows, that at least the spectral lines of $Q_\Lambda(x, y)$ of the length L_Λ live in a p-dimensional subspace with $p \ll L_\Lambda$. Therefore, there is a linear transform E reducing the size of the cube $Q_\Lambda(x, y)$ to the cube of the smaller size. Following [8], we herein term the images associated with this p-dimensional subspace as eigenimages. A smaller size of

978-9-0827-9703-9/19/$31.00 ©2019 IEEE

this subspace automatically means a potential to improve the HSI denoising and to obtain a faster algorithm.

2) *Sparsity* of $2D$ images $U(x,y,\lambda)$ as functions of (x,y) means that there are bases such that $U(x,y,\lambda)$ can be represented with a small number of atoms. It is one of the natural and fundamental assumptions for design of modern image processing algorithms. The sparsity for complex-valued images is quite different from the standard formulation of this concept for real-valued signals. The complex-valued variables can be defined by any of two pairs: amplitude/phase or real/imaginary values and elements of these pairs usually are correlated [5], [9]. Thus, the sparsity can be introduced for different variables: directly for complex-valued or for the real-valued pairs: amplitude/phase or real/imaginary values.
3) The *noise* $\varepsilon_\Lambda(x,y)$ is zero mean circular Gaussian with unknown spectral correlation matrix $L_\Lambda \times L_\Lambda$.

Clean image subspace identification is an important step in the developed algorithm. Estimates of the signal and noise correlation matrices are used to selects p-subspaces of eigen-images that represent the signal subspace in the best least-square error sense.

III. Proposed algorithms

We present and demonstrate two types of the algorithms for HSI: separate and joint denoising of HS images.

A. Separate denoising of HS images

The algorithms of this group filter the images of the hyperspectral cube for each wavelength independently with results which can be shown as

$$\hat{U}(x,y,\lambda) = CDBM3D\{Z(x,y,\lambda)\},\ \lambda \in \Lambda, \qquad (2)$$

where $CDBM3D$ is an abbreviation for Complex Domain Block-Matching 3D filter and $\hat{U}(x,y,\lambda)$ is an estimate of the clean unknown slice $U(x,y,\lambda)$.

Various $CDBM3D$ algorithms are publicly available in MATLAB codes [10], [11].

These algorithms are complex-domain developments of the popular real-valued Block-Matching 3D (BM3D) filters [12]. Two points define the potential advantage of CDBM3D in comparison, in particular, with real-valued BM3D used independently for phase and amplitude as it is in [7], [13]. First, CDBM3D processes phase and amplitude jointly taking into consideration correlation of these variables quite usual in most applications. An independent filtering of amplitude and phase ignores this correlation. Second, the basic functions used for processing of grouped data in BM3D are fixed, while in CDBM3D they are varying data adaptive based on SVD and high-order SVD (HOSVD) of variables.

The both types of the algorithms, BM3D and CDBM3D, are based on nonlocal similarity of small patches of $2D$ images. The algorithms look for the similar patches, say in slices $Z(x,y,\lambda)$, identify them and process together.

A generic CDBM3D algorithm has a structure shown in Fig. 1 composed from two successive stages: thresholding and Wiener filtering. Each of these stages includes: grouping mentioned above, SVD or HOSVD analysis, thresholding or Wiener filtering for the grouped data spectra and aggregations of the filtered spectra to get intermediate and final image estimates.

Following procedure in patch-based image processing, a noisy image $Z(x,y,\lambda) \subset \mathbb{C}^{N\times M}$ taken with a fixed λ is partitioned into small overlapping rectangular/squares $N_1 \times M_1$ patches and this partitioning is produced for each pixel of the image. For each patch, we search in $Z(x,y,\lambda)$ for similar patches, identify them and stack together in $3D$ arrays (tensors). This procedure is called grouping. It follows by HOSVD of these groups defining data-adaptive orthonormal transforms of the complex-valued groups and the core tensors giving the spectral representations of the grouped variables. The next step of the algorithm, as shown in Fig. 1, is filtering implemented as thresholding (zeroing for hard-thresholding) of small items of the core tensors. Inverse HOSVD using the thresholded core tensors returns block-wise estimates of the denoised images. These multiple estimates are aggregated in order to obtain improved image estimates calculated as weighted group-wise mean estimates.

These grouping, HOSVD, thresholding and aggregation define the so-called thresholding filtering. The image filtered by thresholding is an input signal of the second stage of the CDBM3D algorithm - Wiener filtering. The structure of this second part of the algorithm is similar to the thresholding stage with the only difference that the thresholding is replaced by the Wiener filtering.

An output of the Wiener filter is an output of the CDBM3D algorithm. The details of the thresholding and Wiener filtering can be seen in [9]–[11].

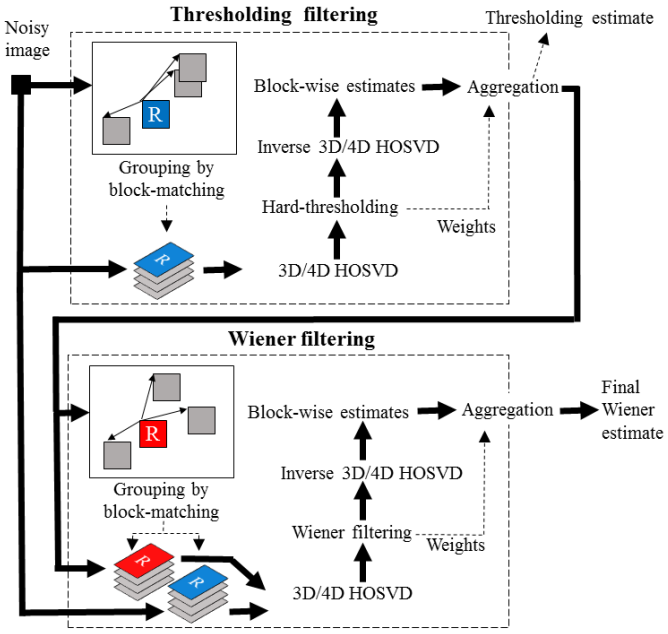

Fig. 1. Flow chart of complex domain BM3D/BM4D filters.

It is demonstrated in [9], [11], that the HOSVD analysis can be produced using instead of complex-valued variables the real-valued pairs amplitude/phase or real/imaginary parts of complex-valued variables. Then, the groups become $4D$ arrays and $4D$ HOSVD is used for the spectral analysis and filtering. The corresponding complex-domain filters are named as CDBM4D. The flow chart in Fig. 1 presents the generic structure of the both types of these algorithms, where we show both $3D$ and $4D$ HOSVD.

The CDBM3D algorithm is originated from [10], where the hard-thresholding filtering is used only and HOSVD is applied to $3D$ groups composed from complex-valued observations. The simulation experiments in this paper are restricted to this single-stage algorithm as the fastest version of CDBM3D.

B. Joint denoising of HS images

This algorithm is developed specially for joint processing of slides of a HS cube and presented in the following notation:

$$\hat{U}_\Lambda(x,y) = \mathcal{CCF}\{Z_\lambda(x,y),\ \lambda \subset \Lambda\}. \tag{3}$$

Complex domain Cube Filter ($\mathcal{CCF}$) processes the data of the cube $Z_\Lambda(x,y)$ jointly and provides the estimates $\hat{U}_\Lambda(x,y)$ for all $\lambda \in \Lambda$.

$\mathcal{CCF}$ is built from the following steps:

1) Reshape $3D$ data cube Z_Λ of size $N \times M \times L_\Lambda$ to the $2D$ matrix Z of the size $L_\Lambda \times NM : N \times M \times L_\Lambda \to L_\Lambda \times NM$;
2) Calculate an orthonormal transform matrix $E \subset \mathbb{C}^{L_\Lambda \times p}$ and $2D$ transform domain eigenimages $Z_{2,eigen}$ for the matrix Z as

$$[E, Z_{2,eigen}, p] = HySime(Z), \tag{4}$$

   where ***HySime*** stays for Hyperspectral signal Subspace Identification by Minimum Error [14].
   HySime is an important part of the $\mathcal{CCF}$ algorithm. It identifies an optimal subspace for the HS image representation including both the dimension of the eigenspace p and eigenvectors - columns of E. When E is given, the eigenimages are calculated as

$$Z_{2,eigen} = E^H Z. \tag{5}$$

3) Reshape the 2D transform domain $Z_{2,eigen}$ of size $p \times MN$ to the 3D image domain array $Z_{3,eigen}$ of size $N \times M \times p : p \times NM \to N \times M \times p$;
4) Filter each of $N \times M$ images (slices) of $Z_{3,eigen}$ by CDBM3D:

$$\hat{Z}_{3,eigen}(x,y,\lambda_s) = CDBM3D(Z_{3,eigen}(x,y,\lambda_s)), \tag{6}$$

   where λ_s identify the images of the eigenspace.
5) Reshape the 3D array $\hat{Z}_{3,eigen}(x,y,\lambda_s)$ to the 2D transform domain $\hat{Z}_{2,eigen}$ of size $p \times NM$ and go back from the eigenimage space to the 2D image space:

$$\hat{Z}_2 = E\hat{Z}_{2,eigen}. \tag{7}$$

   Here E stands for inverse of the p-transform (5).
6) Reshape the 2D image $\hat{Z}_2$ to original HS cube size $N \times M \times L_\Lambda$, it gives the filtered cube $\hat{U}_\Lambda(x,y)$ (3).

These multiple forward and backward passages $2D \leftrightarrows 3D$ allow to define the $2D$ eigenspace $Z_{2,eigen}$ in the p-transform domain and to produce the filtering in the corresponding $3D$ domain $Z_{3,eigen}$. In order to return these filtered data $\hat{Z}_{3,eigen}$ in the original image space, we need to use $2D$ transform (7) and, then, again to reshape $3D$ data into $2D$ space.

The SVD based algorithm ***HySime*** solves the following problems: estimation of noise, estimation of noise covariance matrix and optimization of the signal subspace minimizing mean-square error between the clean HS $U_\Lambda(x,y)$ and its estimate. Note, that the covariance $r_{\lambda,\lambda'}$ in ***HySime*** is obtained by averaging over (x,y) and the preliminary estimate of HS images is used in ***HySime***, which is different from the final HS estimate as defined by (7).

Optimization of the subspace in ***HySime*** results in minimization of its size p and usually $p \ll L_\Lambda$, which simplifies the data processing and leads to the faster algorithm. The CDBM3D filtering is produced only for p eigenimages but the backward transform (7) gives the estimates for all L_Λ spectral images.

The ***HySime*** algorithm for real-valued HSI is derived in [14], where its background and details can be seen.

Our analysis produced for the derivation given in [14] proves that this algorithm is applicable in complex domain within slight modifications concerning a work with complex-valued variables.

Overall, the presented $\mathcal{CCF}$ algorithm follows the structure of the fast denoising algorithm derived for real-valued HSI [8]. The principal difference between our and this algorithm is in the filters used for denoising: real domain BM3D in ***FastHyDe*** and complex domain CDBM3D in $\mathcal{CCF}$.

IV. Simulation experiments

Simulation experiments are produced for the complex-valued wavefronts obtained from propagation of HS coherent beam through thin transparent object. Then, the phase delay is proportional to the thickness of the object and calculated in radians as

$$\varphi(x,y) = 2\pi \frac{h(x,y)}{\lambda}(n_\lambda - 1), \tag{8}$$

where λ is a wavelength of the wavefront ($\Lambda = 400 - 800$ nm) with total number of slices $L_\Lambda = 200$, $h(x,y)$ is an object's thickness, and n_λ is the refractive index of optical material of the object.

The clean HS cube is calculated as

$$Q_\Lambda(x,y) = \{U(x,y,\lambda), \lambda \subset \Lambda\}, \tag{9}$$

where $U(x,y,\lambda)$=$A(x,y) \cdot \exp(j\varphi(x,y))$.

For simplicity, we assume totally transparent object, that means that the amplitude $A(x,y)$ of HS wavefronts is equal to 1, i.e. optical absorption of the object is negligible.

The function $h(x,y)$ is a two-peak surface illustrated in Fig. 2(a, b) by the absolute and wrapped phases φ for the wavelength $\lambda = 598$ nm, correspondingly. The additive Gaussian noise power is described by standard deviation σ.

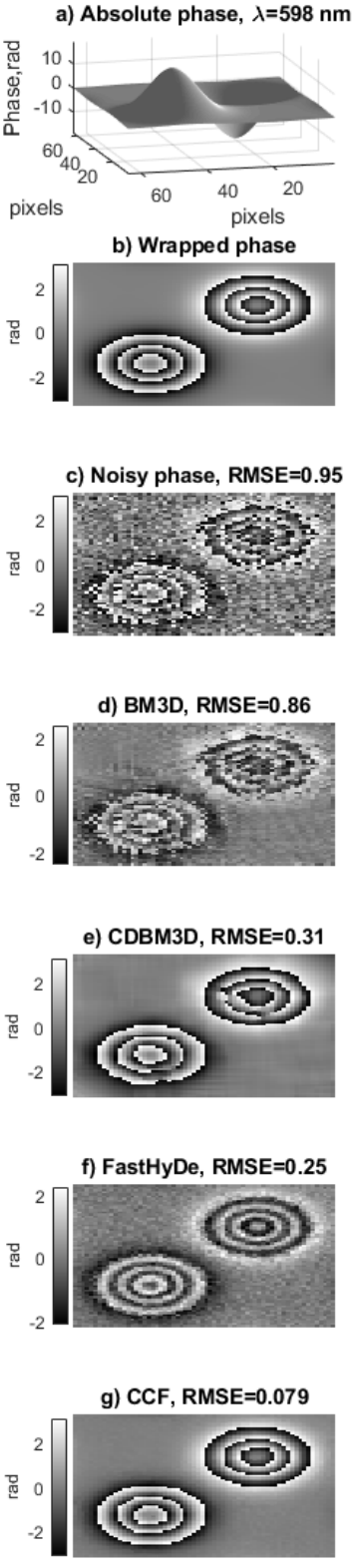

Fig. 2. Object and filtered phases. Clear absolute (a) and wrapped object phases (b), noisy observed phase (c), wrapped phase reconstructions by the $BM3D$ (d), $CDBM3D$ (e), $FastHyDe$ (f), and $\mathcal{CCF}$ (g) algorithms. The visual and numerical advantage of $\mathcal{CCF}$ is obvious.

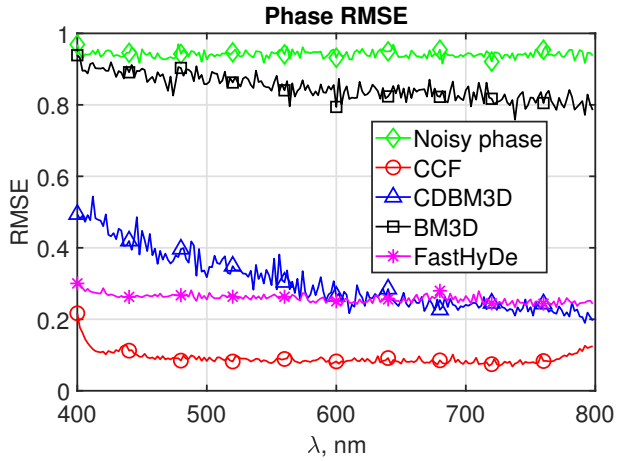

Fig. 3. Distribution of RMSEs over wavelengths for the compared algorithms: curve with squares (black) is for BM3D, with triangles (blue) for CDBM3D, with stars (magenta) for FastHyDe, with circles (red) for $\mathcal{CCF}$. The upper nearly horizontal curve with diamonds (green) is for the observed noisy phase provided $\sigma = 0.3\pi$. FastHyDe, magenta curve with stars, demonstrates performance closest to $\mathcal{CCF}$ but with a valuable advantage of the latter.

We compare the $\mathcal{CCF}$ algorithm versus CDBM3D, where the slices $Z(x, y, \lambda)$ are processed independently in the complex domain, and versus BM3D where the real domain filtering produced for phase and amplitude independently. Additionally, a comparison versus FastHyDe [8] applied to the real-valued cube of the noisy phases calculated for noisy observations Eq.(1) is presented. The results are shown in Figs. 2 - 4.

Figs. 2 and 3 provide a visual and numerical comparison of the algorithms with a fixed value of the noise standard deviation $\sigma = 0.3\pi$, while Fig. 4 shows RMSE values as functions of σ.

Fig. 2(d) illustrates filtering of a noisy wrapped phase of the slice $Z(x, y, \lambda)$ by BM3D. The results for the more advanced CDBM3D and the proposed $\mathcal{CCF}$ are shown in Fig. 2 (e) and Fig. 2 (g), respectively. In Fig. 2 (f), we can see the results obtained by FastHyDe. The visual advantage of the $\mathcal{CCF}$ algorithm is obvious and supported by the lowest value of RMSE equal to 0.079.

RMSE curves for the each filtering algorithm and for the observed noisy phase are presented in Fig. 3 as functions of λ, $\sigma = 0.3\pi$. The curve with diamonds (green) presents RMSE for the noisy phase of the observations. These RMSE values close to 1 correspond to a very noisy case with a hardly distinguishable phase of the object. The curve with squares (black) is RMSE for BM3D filtering, its' values are close to 1 also, which means that the separate phase/amplitude BM3D filtering is not effective for such complex data. The curve with triangles (blue) is for the CDBM3D algorithm. It demonstrates a significant improvement of filtering in comparison with BM3D, but nevertheless, it lost some details of the object image.

The curve with circles (red) is for the $\mathcal{CCF}$ algorithm with RMSE values about 0.1 corresponding to a very good noise suppression and an appropriate revealing of the object details.

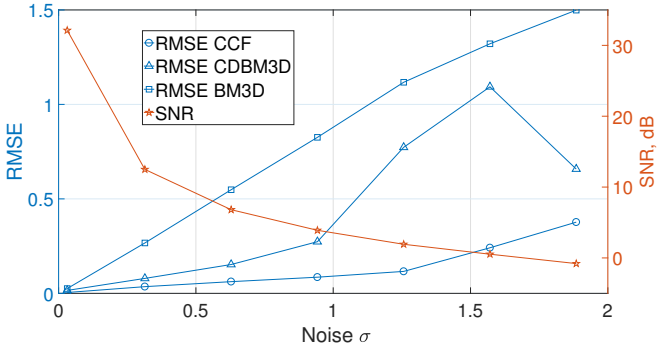

Fig. 4. RMSE values for different values of the noise standard deviation and SNR for observations.

An inclination of the RMSE curves for BM3D and CDBM3D to smaller values for larger wavelengths λ in Fig. 3 is explained as a better filtering for the data slices with smaller ranges of the absolute phases, which corresponds to flatter surfaces of the corresponding wrapped phases. Such inclination is not observed for the $\mathcal{CCF}$ algorithm since $\mathcal{CCF}$ takes into account all slices of HS cube and filtering quality is limited by the whole HS cube $Z(x, y, \Lambda)$ but not separate slices $Z(x, y, \lambda)$.

FastHyDe, magenta curve with stars, demonstrates performance which is much better than that shown by BM3D and CDBM3D because this algorithm process all data of the cube simultaneously but being applied to the phase data present the much lower accuracy than $\mathcal{CCF}$.

Fig. 4 is a double Y-axis graph, where the left Y-axis is for RMSE and the right Y-axis is for signal-to-noise ratio (SNR) calculated for noisy phase data, $\lambda = 598$ nm. Naturally, all RMSE curves are growing functions of σ. RMSE for $\mathcal{CCF}$ (blue circles) take smallest values, what confirms the best performance of the proposed algorithm versus BM3D and CDBM3D, and reliable $\mathcal{CCF}$ results are obtained even for extremely noisy data, $SNR \approx 2$, with RMSE $= 0.11$.

For our simulation experiments, we use MATLAB R2017b and the computer with the processor Intel(R) Core(TM) i7-3770 CPU @ 3.40 GHz, 32 Gb RAM. The computation complexity of the algorithm is characterized by the time required for processing. For $64 \times 64 \times 200$ HS cube, it is equal to 12 sec.

V. Conclusion

In this paper, we present the algorithm for denoising of 3D HS complex-valued data cube. In simulation experiments, the algorithm demonstrates the state-of-the-art performance visually and numerically owing to the SVD analysis of noisy HS observations and CDBM3D filtering in the SVD eigenspace. The outstanding noise suppression and object detail preservation are due to joint processing of 2D slices of 3D HS data. Such good results cannot be achieved by separate denoising of 2D slices of HS observations even using the high-accuracy BM3D and CDBM3D algorithms or by joint processing of real-valued slices, as it shown in this paper for the phase cube filtering by the FastHyDe algorithm. The proposed algorithm is efficient and stable even for low SNR observations.

The MATLAB demo-codes of the proposed algorithm will be publicly available on the website: http://www.cs.tut.fi/sgn/imaging/sparse/.

References

[1] M. J. Khan, H. S. Khan, A. Yousaf, K. Khurshid, and A. Abbas, "Modern Trends in Hyperspectral Image Analysis: A Review," pp. 14 118–14 129, 2018.

[2] G. Lu and B. Fei, "Medical hyperspectral imaging: a review," *Journal of Biomedical Optics*, vol. 19, no. 1, p. 010901, 2014.

[3] M. S. Kulya, V. A. Semenova, V. G. Bespalov, and N. V. Petrov, "On terahertz pulsed broadband Gauss-Bessel beam free-space propagation," *Scientific Reports*, vol. 8, no. 1, p. 1390, 12 2018.

[4] D. B. Rowe, "Modeling both the magnitude and phase of complex-valued fMRI data," *NeuroImage*, vol. 25, no. 4, pp. 1310–1324, 2005.

[5] S. G. Kalenkov, G. S. Kalenkov, and A. E. Shtanko, "Hyperspectral holography: an alternative application of the Fourier transform spectrometer," *Journal of the Optical Society of America B*, vol. 34, no. 5, p. B49, 2017.

[6] D. Claus, G. Pedrini, D. Buchta, and W. Osten, "Accuracy enhanced and synthetic wavelength adjustable optical metrology via spectrally resolved digital holography," *Journal of the Optical Society of America A: Optics and Image Science, and Vision*, vol. 35, no. 4, pp. 546–552, 2018.

[7] G. S. Kalenkov, S. G. Kalenkov, I. G. Meerovich, A. E. Shtanko, and N. Y. Zaalishvili, "Hyperspectral holographic microscopy of bio-objects based on a modified Linnik interferometer," *Laser Physics*, vol. 29, no. 1, p. 016201, 1 2019.

[8] L. Zhuang and J. M. Bioucas-Dias, "Fast Hyperspectral Image Denoising and Inpainting Based on Low-Rank and Sparse Representations," *IEEE Journal of Selected Topics in Applied Earth Observations and Remote Sensing*, vol. 11, no. 3, pp. 730–742, 3 2018.

[9] V. Katkovnik, M. Ponomarenko, and K. Egiazarian, "Sparse approximations in complex domain based on BM3D modeling," *Signal Processing*, vol. 141, pp. 96–108, 12 2017.

[10] V. Katkovnik and K. Egiazarian, "Sparse phase imaging based on complex domain nonlocal BM3D techniques," *Digital Signal Processing: A Review Journal*, vol. 63, pp. 72–85, 4 2017.

[11] V. Katkovnik, M. Ponomarenko, and K. Egiazarian, "Complex-valued image denosing based on group-wise complex-domain sparsity," *arxiv*, vol. 1711.00362, 11 2017.

[12] K. Dabov, A. Foi, V. Katkovnik, and K. Egiazarian, "Image Denoising by Sparse 3-D Transform-Domain Collaborative Filtering," *IEEE Transactions on Image Processing*, vol. 16, no. 8, pp. 2080–2095, 8 2007.

[13] V. Katkovnik and J. Astola, "Phase retrieval via spatial light modulator phase modulation in 4f optical setup: numerical inverse imaging with sparse regularization for phase and amplitude," *Journal of the Optical Society of America A*, vol. 29, no. 1, p. 105, 2012.

[14] J. M. Bioucas-Dias and J. M. Nascimento, "Hyperspectral subspace identification," *IEEE Transactions on Geoscience and Remote Sensing*, vol. 46, no. 8, pp. 2435–2445, 2008.